

Expression of GPX4 by oncolytic vaccinia virus can significantly enhance CD8⁺T cell function and its impact against pancreatic ductal adenocarcinoma

Wei Wei^a, Linqing Tian^b, Xiaoyan Zheng^c, Lei Zhong^d, Yuan Chen^e, Hui Dong^f, Guibing Zhang^g, Shibing Wang^h, and Xiangmin Tongⁱ

^aZhejiang Provincial People's Hospital Affiliated People's Hospital, Hangzhou Medical College, Postgraduate Training Base of Jinzhou Medical University, Hangzhou, Zhejiang, People's Republic of China; ^bDepartment of Clinical Medicine, Bengbu Medical College, Bengbu, China; ^cDepartment of Laboratory Medicine, Quzhou Affiliated Hospital of Wenzhou Medical University, Quzhou People's Hospital, Quzhou, Zhejiang, China; ^dDepartment of Laboratory Medicine, Tongxiang Traditional Chinese Medicine Hospital, Tongxiang, Zhejiang, China; ^eDepartment of Pathology, Zhejiang Provincial People's Hospital Affiliated People's Hospital, Hangzhou Medical College, Hangzhou, Zhejiang, China; ^fDepartment of Stomatology, Punan Hospital of Pudong New District, Shanghai, China; ^gDepartment of Hematology, Hangzhou Fuyang First People's Hospital, Hangzhou, Zhejiang, People's Republic of China; ^hCancer Center, Department of Pathology, Zhejiang Provincial People's Hospital Affiliated People's Hospital, Hangzhou Medical College, Hangzhou, Zhejiang, China; ⁱKey Laboratory of Integrated Oncology and Intelligent Medicine of Zhejiang Province, Department of Clinical Research Center, Affiliated Hangzhou First People's Hospital, Zhejiang University School of Medicine, Hangzhou, Zhejiang, China

ABSTRACT

Pancreatic ductal adenocarcinoma (PDAC) is currently difficult to treat, even when therapies are combined with immune checkpoint blockade (ICB). A novel strategy for immunotherapy would be to maximize the therapeutic potential of oncolytic viruses (OVs), which have been proven to engage the regulation of tumor microenvironment (TME) and cause-specific T-cell responses. To boost tumor sensitivity to ICB therapy, this study aimed to investigate how glutathione peroxidase 4 (GPX4)-loaded OVs affect CD8⁺ T cells and repair the immunosuppressive environment. Here, we successfully constructed a novel recombinant oncolytic vaccinia virus (OVV) encoding the mouse GPX4 gene. We found the OVV-GPX4 effectively replicated in tumor cells and prompted the expression of GPX4 in T cells. Our research indicated that OVV-GPX4 could reshape the TME, rectify the depletion of CD8⁺T cells, and enhance the antitumor effects of ICB therapy.

ARTICLE HISTORY

Received 26 October 2023
Revised 18 February 2024
Accepted 19 February 2024

KEYWORDS

Glutathione peroxidase 4; oncolytic vaccinia virus; pancreatic ductal adenocarcinoma; tumor microenvironment

Introduction


Pancreatic ductal adenocarcinoma (PDAC) is a fatal gastrointestinal tumor with a 5-year survival rate of 12%.¹ Only 11% of patients are diagnosed when the disease first appears locally, and 52% of PDACs are metastatic when detected, resulting in a high death rate.² Its difficult-to-access anatomical position, the absence of biomarkers for its early identification, and asymptomatic or unrecognized localized conditions make diagnosis difficult. Surgical resection combined with radiotherapy and chemotherapy are the conventional treatments for PDAC.^{1,2} Farren et al. investigated the total and spatial expression of immune-related transcripts and proteins in the tumor microenvironment (TME) of PDAC patients and found that immune-related genes were differentially regulated by different treatments.³

In addition to conventional treatments, immunotherapies to alter the TME of PDAC are essential and promising. Only a tiny proportion of the TME comprises cancer cells, but its increased fibroblast population, dense extracellular matrix, poor vascularization, and immunosuppressive cells drive its invasiveness, heterogeneity, and drug resistance.⁴

A prominent feature of PDAC “cold” tumors is the absence of CD8⁺ T lymphocytes and the low activation markers.^{5,6} Immune checkpoint blockade (ICB) treatments targeting CTLA-4 or PD-1/PD-L1 have limited effectiveness in PDAC, a phenomenon that may be attributable to the scarcity of T cells in these tumors.^{7–9}

Oncolytic viruses (OVs) are promising cancer treatments because they can lyse tumor cells while activating the innate and adaptive immune systems, accumulate tumor-infiltrating lymphocytes (TILs) and transform immunological “cold” tumors into “hot”.^{10,11} Recently, researchers have modified OV vectors to boost their anti-tumor effects.^{11,12} This is accomplished by equipping co-stimulatory molecules to enhance the ability of antigen-presenting cells.^{13–15} Additionally, armed chemokines^{16,17} and cytokines^{18,19} attract lymphocytes and boost anti-tumor activity. Added tumor-related antigens²⁰ can facilitate adaptive immunity, while immune checkpoint inhibitors^{21,22} alleviate immunosuppression. OVs offer the potential to utilize adoptive T cells as vehicles for treating secondary tumors,²³ virus particles can adhere to the surface of T cells or internalize into T cell

CONTACT Shibing Wang  wangshibing@hmc.edu.cn  Cancer Center, Department of Pathology, Zhejiang Provincial People's Hospital (Affiliated People's Hospital, Hangzhou Medical College), Hangzhou, Zhejiang 310014, China; Xiangmin Tong  tongxiangmin@163.com  Key Laboratory of Integrated Oncology and Intelligent Medicine of Zhejiang Province, Department of Clinical Research Center, Affiliated Hangzhou First People's Hospital, Zhejiang University School of Medicine, Hangzhou, Zhejiang 310006, China

 Supplemental data for this article can be accessed online at <https://doi.org/10.1080/2162402X.2024.2322173>.

© 2024 The Author(s). Published with license by Taylor & Francis Group, LLC.

This is an Open Access article distributed under the terms of the Creative Commons Attribution-NonCommercial License (<http://creativecommons.org/licenses/by-nc/4.0/>), which permits unrestricted non-commercial use, distribution, and reproduction in any medium, provided the original work is properly cited. The terms on which this article has been published allow the posting of the Accepted Manuscript in a repository by the author(s) or with their consent.

compartments.²⁴ Recent research has indicated that myxoma virus-infected CAR-T and TCR-T cells could induce tumor cells autolysis²⁵ and infected cell carriers exhibited greater resilience against antiviral immunity.²⁶ T-cell engager-armed oncolytic vaccinia virus (OVV) was also verified to enhance antitumor therapy significantly.²⁷

Glutathione peroxidase 4 (GPX4) has been identified as the central regulatory factor of ferroptosis, catalyzing the reduction of lipid peroxides. The absence of GPX4 would lead to cell death from lipid peroxidation.²⁸ Although GPX4 inhibitors exhibit great potential for inhibiting cancer cells via ferroptosis, the sensitivity of distinct tumor cell lines to it varied considerably.²⁹ Conventional GPX4 inhibitors have notable deficiencies, including inadequate pharmacokinetics, limited selectivity,³⁰ and remarkable sensitivity toward CD8⁺T cells. At concentrations that do not impact the quantity of B16 melanoma or MC38 colorectal cancer cells, GPX4 inhibitors stimulate ferroptosis in CD8⁺T cells via lipid peroxidation, diminishing their survival.³¹ Therefore, the application of GPX4 inhibitors in tumor therapy is severely restricted. Immune cell phenotype and function are influenced by TME lipid metabolism changes. T regulatory cells (Tregs), regulatory B cells, M2 macrophages, myeloid-derived suppressor cells (MDSCs), and N2 neutrophils are inclined to exercise their immunosuppressive capacity inside tumors through lipid metabolism.³² Effector T cells prefer glycolysis and aerobic respiration to get their ATP,³³ but passively absorbing harmful lipids like oxidized low-density lipoprotein (ox-LDL) affects their cytokine secretion and mortality.^{32–34} GPX4 maintains homeostasis by degrading toxic lipid peroxides^{28,35} and is closely related to CD36,³⁶ which regulates lipid uptake and metabolism. Studies show that increasing CD36 on CD8⁺T cells in TME is linked to tumor progression and poor prognosis. CD36-deficient mice have more CD8⁺ effector T cells and GPX4 mRNA in their TILs, delaying tumor growth.^{37,38} Transduction of GPX4-overexpressing retroviruses into T cells can reduce lipid peroxidation and increase IFN- γ and TNF- α production, enhancing antitumor effects.³⁸

This study proposed to exert the ability of OVV to lyse tumor cells while increasing GPX4 expression in effector T cells to reduce lipid peroxidation, reverse T-cell depletion, and alleviate the immunosuppressive microenvironment. We also aimed to use the OVV platform with ICB to create a synergistic effect and investigate treatment mechanisms.

Materials and methods

Cell lines and cell culture

The American Type Culture Collection (ATCC; Manassas, USA) provided the cell lines HEK293 (CRL-1573), Hela-S3 (CCL-2.2), Vero (CCL-81), Panc02(CRL-2553), CT26 (CRL-2638) and Hepa1–6(CRL-1830). MC38 cell line was stored in our lab. All cells were incubated in DMEM (Gibco Thermo Fisher Scientific, USA, Cat # 11965092) with 10% FBS (Gibco Cat # 16000044) at 37°C and 5% CO₂.

Recombinant OVV construction

GenScript (Nanjing, China) produced the GPX4 gene fragment, which was then subcloned into the shuttle plasmid pVV-Control to create the recombinant plasmid pVV-GPX4. In this plasmid, GPX4 is expressed by a synthetic early/late promoter (pSE/L), whereas enhanced green fluorescent protein (EGFP) and guanine-hypoxanthine phosphoribosyl transferase (GPT) are expressed by a VV p7.5K early/late promoter. To generate OVV-GPX4, the shuttle plasmid pVV-GPX4 was homologously recombined with a western reserve strain of VV (WR-VV; VR-1354; ATCC). In brief, HEK293 cells were infected for 2 h with the WR-VV at a MOI of 1 before being transfected with the pVV-GPX4 using the lipofectamine transfection reagent (Cat#A12621, ThermoFisher). The EGFP-positive plaques were chosen and 48 hours later planted in plates containing Hela-S3 cells. A conditional DMEM medium containing 250 g/mL xanthine (Cat#A601197, Sangon Biotech, Shanghai, China), 25 g/mL mycophenolic acid (Cat#A600640, Sangon), and 15 g/mL hypoxanthine (Cat#A500336, Sangon) was used to limit the growth of WR-VV. PCR and DNA sequencing were done after many picking and seeding cycles to demonstrate that the recombinant virus was no longer infected with WR-VV. The purified virus was then grown in 6-well plates, cell culture dishes, and cell culture spinner flasks by Hela-S3 cells. The virus titer was determined using the TCID50 method. The following is the calculating formula: Virus titer = $0.7 \times 10 \times 10^{(1+S(D-0.5))}$, where S is log₁₀ (dilution) and D is the total of the positive EGFP ratios in each dilution.

Western blot

Protein samples were obtained from Vero cell lysates or supernatants that were infected with either OVV or OVV-GPX4. The instructions of BCA assay kit (Cat#23227, Thermo) were followed to measure protein concentrations in the samples. Protein samples were separated on a 10–15% SDS/PAGE gel and transferred to a PVDF membrane. The proteins were detected by GPX4 Monoclonal antibody (Cat# 67763–1-Ig, Proteintech). Then, the imprint was detected in one hour with the second antibody (Cat# HA1001, Hua'an Biotechnology).

CCK8 assay

Panc02, CT26, MC38, and Hepa 1–6 cells were cultured at 5×10^3 cells per well in 96-well plates and then infected with OVV or OVV-GPX4 at designated MOIs (0.005, 0.05, 0.5, 5) in triplicate. After 48 hours of incubation, CCK8 solution (Cat# C0037, Beyotime) was added 10 μ l to each well and incubated for an additional hour. Molecular Devices Spectra Max M3 was used to measure 450 nm absorbance. Cell viability can be calculated using this equation: Cell viability (%) = (A treatment - blank)/(A control - blank) \times 100%.

The infectivity of oncolytic vaccinia virus in tumor cells

Tumor cells (Panc02, CT26, MC38, and Hepa1–6) were infected in a 24-well plate at 5×10^4 cells per well with recombinant OVV and OVV-GPX4-GFP at 0.1 MOIs in a 5% CO₂ and 37°C incubator. Cells were collected after 24, 48, 72, and

96 hours, centrifuged at 300×g for 3 minutes. The percentage of infected cells was detected by the FITC channel of flow cytometry (NovoCyte Quanteon, Agilent).

Peripheral blood mononuclear cells (PBMCs) preparation and T cell isolation

The Ethics Committee of Zhejiang Provincial People's Hospital has approved all animal studies conducted. C57BL/6 mouse blood was collected. PBMCs were separated by Ficoll density gradient centrifugation. These cells were resuspended in 10% FBS AIMV (Cat# 087-0112DK, Gibco) media. T cells were isolated by the Pan T cell Isolation kit (Cat# 130-095-130, MiltenyiBiotec) from PBMCs. Subsequently, these cells were resuspended with IL-2 (300 IU/ml), IL-7 (5 ng/ml), and IL-15 (5 ng/ml) (Prime Gene). T-activator CD3/CD28 (Cat#11456D, Gibco) was added to activate T cells.

The expression of GPX4 in T cells by real-time quantitative polymerase chain reaction (RT-qPCR)

After co-incubation of OVV, OVV-GPX4 (MOI = 10) or PBS with isolated T cells for 48 hours, centrifuged 400×g for 3 minutes and collected cell precipitates. The RNA samples were obtained through the utilization of the FastPure Cell/Tissue Total RNA Isolation Kit (Cat# RC101-01, Vazyme Biotech) to eliminate any presence of genomic DNA. Reverse transcription was performed using HiScript II Reverse Transcriptase (Cat# R201-01, Vazyme Biotech) on a sample of RNA (1 µg). 40 ng complementary DNA (cDNA) was utilized for quantification. Real-time analysis was performed in 7500 Fast Real-Time PCR System according to HiScript III RT SuperMix for qPCR (+gDNA wiper) (Cat# R323, Vazyme Biotech). The PCR conditions were: 40 cycles at 95°C for 10 minutes, 95°C for 15 seconds, 60°C for 1 minute, and 72°C for 7 minutes. The primers used in the experiment were:

Gpx4-F: 5'-GAGGCCAAACTGACGTAAACTACAC-3'
Gpx4-R: 5'-TCTTGATTACTTCCTGGCTCCTG-3'

T cell in vitro by flow cytometry analysis

Isolated T cells were labeled with carboxy fluorescein succinimidyl ester (CFSE) fluorescent dye (Cat# C1031, Beyotime), cocultured with Panc02 cells at a ratio of 6:1 (CD3⁺T: Panc02 cells), and added OVV, OVV-GPX4 viral supernatant (MOI = 10) or PBS. After 48 hours, the proliferation of T cells was tested by flow cytometry. In other parallel experiments, T cells were cocultured with OVV, OVV-GPX4 viral supernatant (MOI = 10) or PBS for 48 h. T cells suspension was stained with the following antibodies: anti-CD8 (Cat# 100706, Biolegend), anti-CD25 (Cat# 102021, Biolegend), anti-CD36 (Cat# 102611, Biolegend) and Bodipy 581/591 C11 (Cat# D3861, Invitrogen).

Establishment of syngeneic mice models

Panc02 cells were subcutaneously injected at a concentration of 1.5×10^6 cells per 100 µl into C57BL/6 mice that were 5 weeks old. In the investigation of in vivo anti-tumor effects, following the establishment of tumors, we administered intratumoral

injections of phosphate-buffered saline (PBS), OVV, OVV-GPX4 at a dosage of 2×10^7 plaque-forming units (pfu)/mouse or GPX4 protein (1 µg/mouse) for five times. In parallel experiments to depleted CD8⁺ and CD4⁺ T cells, we administered PBS, OVV-GPX4, OVV-GPX4 combined with anti-CD8 or anti-CD4 antibody alone. The infection of OVV-GPX4 (2×10^7 pfu/mouse) or PBS was at day 0,2,4,6,8 and anti-CD8 or anti-CD4 antibody (100 µg/mouse) at day 3,5,7. To test the combined effect with anti-PD-1 antibodies, Panc02 models were injected with PBS or OVV-GPX4 (2×10^7 pfu/mouse) alone at day 0,2,4,6,8 and anti-PD-1 antibody on day 1,3,5,7,9. To verify abscopal effect, the mice were bilaterally inoculated with Panc02 cells on the right flank (1.5×10^6 cells) and left flank (7.5×10^5 cells) by subcutaneous injection on day -5. Then mice were injected OVV, OVV-GPX4 (2×10^7 pfu/mouse) or PBS for five times on the right flank. Subcutaneous tumor volume was determined by measuring their diameter with a digital caliper. To calculate tumor volume, use the formula: volume = length × width × width × 0.5. All animals must have their tumors measured consistently.

In the investigation for flow cytometry analysis, the intratumoral injections of PBS, OVV, OVV-GPX4 (2×10^7 pfu/mouse) or GPX4 protein (1 µg/mouse) was repeated three times, with a two-day interval between each injection. The mice's tumors and spleens were then collected for analysis 2 days after the injection.

Immune microenvironment and systemic immunity in vivo by flow cytometry analysis

Fresh tumor and spleen samples were minced, treated with 200 U/ml Collagenase I (Cat#ST2294, Beyotime Biotechnology), and filtered with a 100 µm filter to make a suspension of single cells. 2×10^6 Cells were stained at 100 µl in PBS. Single-cell suspension is stained with the following antibodies: Live/Dead Fixable Violet Dead Cell (Cat# 2549272, Invitrogen), anti-CD3 (Cat# 100236, Biolegend), anti-CD4 (Cat# 100406; 100408, Biolegend), anti-CD8 (Cat# 100706, Biolegend), anti-Ki67 (Cat# 652425, Biolegend), anti-IFN-γ (Cat# 505860, Biolegend), anti-Perforin (Cat# 154306, Biolegend), anti-Foxp3 (Cat# 126404, Biolegend), anti-CD11b (Cat# 101212, Biolegend), anti-CD11c (Cat# 117352, Biolegend), anti-Gr-1 (Cat# 108406, Biolegend), anti-TIM-3 (Cat# 119727, Biolegend), anti-LAG-3 (Cat# 125241, Biolegend) and anti-PD-1 (Cat# 135227, Biolegend). Surface antigens were detected by NovoCyte Quanteon (Agilent) after staining with antibodies for 30 minutes in the dark. To detect intracellular cytokines, the samples were fixed with Fixation/Permeabilization Solution KiT (Cat# 554714, BD Biosciences) and incubated with intracellular antibodies for 30 minutes before running the machine. Datas were analyzed by NovoExpress.

Immunohistochemistry (IHC)

Successfully constructed the Panc02 model as described above, we administered intratumoral injections of PBS, OVV, OVV-GPX4 (2×10^7 pfu/mouse) or GPX4 protein (1 µg/mouse) for three times. The injection interval was one day. After injection, the tumor tissues of mice were extracted and soaked in 4%

paraformaldehyde solution. Paraffin-embedded 3–5 mm sections were deparaffinized and hydrated. Samples were steamed at 95°C for 20 minutes in a pH 9.0 Tris-EDTA buffer to retrieve antigens. A hydrophobic barrier was created around tissue sections with a Pap pen. The sections were incubated with 3% H₂O₂ in PBS for 15 minutes. Slides were blocked in 1.5% bovine serum albumin in PBST (0.1% Tween 20) for 30 minutes. The sections were incubated with blocking buffer-diluted CD8 (Cat# 85336S, Cell Signalling, 1:300) primary antibodies. The incubation process lasted overnight at 4°C or 3 hours at room temperature. The slides were incubated with biotinylated anti-rabbit secondary antibodies (Cat#BA-1000, Vector Laboratories, 1:250) for 30 minutes for CD8 immunohistochemistry. After Diaminobenzidine dyeing, slides were counterstained with hematoxylin. Recorded and analyzed images by microscope (Nikon eclipse 100).

RNA sequencing (RNA-seq)

TRIzol (Cat#:15596018, Invitrogen) was used to isolate and purify total RNA from mouse tumor tissues. RNA integrity was assessed by denatured agarose gel electrophoresis. After fragmentation, complementary DNA from poly (A) RNA was created by SuperScript II Reverse Transcriptase (Cat#:1896649, Invitrogen). PCR amplified interconnected products after pretreatment. The final cDNA library inserted averages 300 ± 50 base pairs. Total RNA was extracted, purified, library, and sequenced by LC-Bio Technology. The PE150 sequencing mode was chosen and paired sequencing was conducted by the Illumina Novaseq 6000 platform in accordance with established protocols.

TME in vivo by RT-qPCR

In liquid nitrogen, frozen mouse tissues were broken by mortar and pestle. To detect virus enrichment in different tissues, viral DNA was extracted from a 25 mg homogenate tissue sample by Viral DNA/RNA Kit (Cat#: CW0548S, Cowin Biotech). To detect chemokines, cytokines and co-stimulatory molecules in tumors, RNA was extracted by FastPure Cell/Tissue Total RNA Isolation Kit (Cat# RC101-01, Vazyme Biotech). A 1 µg RNA sample was reverse transcribed using HiScript II Reverse Transcriptase (Cat# R201-01, Vazyme Biotech) to cDNA. The 100 ng DNA viral genome and 40 ng cDNA were used for quantification. Real-time analysis was performed in 7500 Fast Real-Time PCR System according to HiScript III RT SuperMix for qPCR (+gDNA wiper) (Cat# R323, Vazyme Biotech). The PCR conditions were: 40 cycles at 95°C for 10 minutes, 95°C for 15 seconds, 60°C for 1 minute, and 72°C for 7 minutes. The primers used in the experiment were:

C11-F:5'-AAACACACACTGAGAAACAGCATAAA-3'
 C11-R:5'-ACTCGGCGAATGATCTGATTA-3'
 CXCL9-F:5'-ACGGAGATCAAACCTGCCTAGAT-3'
 CXCL9-R:5'-TCAGGGTGCTTGTGGTAAAGTA-3'
 CXCL10-F:5'-GTGTTGAGATCATTGCCACGATG-3'
 CXCL10-R:5'-TCAGAAGACCAAGGGCAATTAGG-3'
 CCL4-F:5'-CCTCCCACTTCTGCTGTTT-3'
 CCL4-R:5'-ACTCCAAGTCACTCATGTAICTCAG-3'
 CXCL13-F:5'-GGTGTCTGGAGTGATTTCAACTG-3'
 CXCL13-R:5'-ATTTGGCACGAGGATTCACACAT-3'
 CD28-F:5'-AGTGACAGTGGCTCTTTGTGTTA-3'

CD28-R:5'-GCAGTGATGATGAGCAGGTAGAC-3'
 ICOS-F:5'-TTACTTCTGCAGCCTGTCCATTT-3'
 ICOS-R:5'-TCATGCACACTGGATCCGTATTT-3'
 GZMB-F:5'-AAAGACCAAACGTGCTTCCTTTC-3'
 GZMB-R:5'-AGCTCTAGGGACGATGGGTAATC-3'
 GAPDH-F: 5'-GGAGCGAGATCCCTCCAAAAT-3'
 GAPDH-R: 5'-GGCTGTTGTCATACTTCTCATGG-3'

Statistical analysis

The GraphPad Prism was used for statistical analysis. Continuous data was represented by mean and standard deviation (SD). These dates compared by unpaired two-tailed Student's t-test or two-way ANOVAs with Tukey's multiple comparison tests. The Kaplan-Meier curve is employed for the assessment of survival outcomes. The typical significance threshold is $p < 0.05$.

Results

GPX4 expression by the oncolytic vaccinia virus

Figure 1a depicted the design of a novel OVV in which the GPX4 gene was inserted at the thymidine kinase (TK) gene deletion site under the control of Pse/L and a green fluorescent gene was added. Western blotting on the OVV-GPX4-infected Vero cell lysates and supernatants showed that OVV-GPX4 increased intracellular and extracellular GPX4 levels (Figure 1b). These results showed that OVV-GPX4 produced and released GPX4.

To determine whether insertion of the GPX4 gene influenced the cytotoxicity and infectivity of the virus, we infected four cell lines (Panc02, CT26, MC38, and Hepa 1–6) for 48 hours with GFP-expressing OVV and OVV-GPX4. In Figure 1c, OVV and OVV-GPX4 had similar cytotoxic effects on tumor cell lines at different MOIs. By flow cytometry, the similar proportion of tumor cells carried fluorescence indicated that there was no significant difference in the infectivity of OVV and OVV-GPX4 (Figure 1d). These cytotoxicity and infectivity experiments showed that GPX4 gene insertion did not affect the cytotoxicity and infectivity of virus.

Effect of OVV-GPX4 on T cells in vitro

To assess how OVV-GPX4 impacts T cells, the CD3⁺T cells were labeled with carboxy fluorescein succinimidyl ester (CFSE) fluorescent dye,³⁹ co-cultured with Panc02 cells at a ratio of 6:1 (CD3⁺T: Panc02 cells), and added OVV or OVV-GPX4 viral supernatant. As depicted in Figure 2a,b CD3⁺T cells in the OVV-GPX4 group demonstrated a greater capacity for proliferation. T cells were also incubated with PBS, OVV, and OVV-GPX4 (MOI = 10) for 48 hours. We found GPX4 transcription increased significantly in the OVV-GPX4 group by qPCR (Figure 2c), confirming that OVV-GPX4 could significantly promote the expression of GPX4 in T cells. During the co-incubation for 24 and 48 hours, there was an elevation in activation marker CD25⁺ on CD8⁺T cells (Figure 2d).

We subsequently utilized flow cytometry to detect CD36, a lipid metabolism protein, on the surface of CD8⁺ T cells

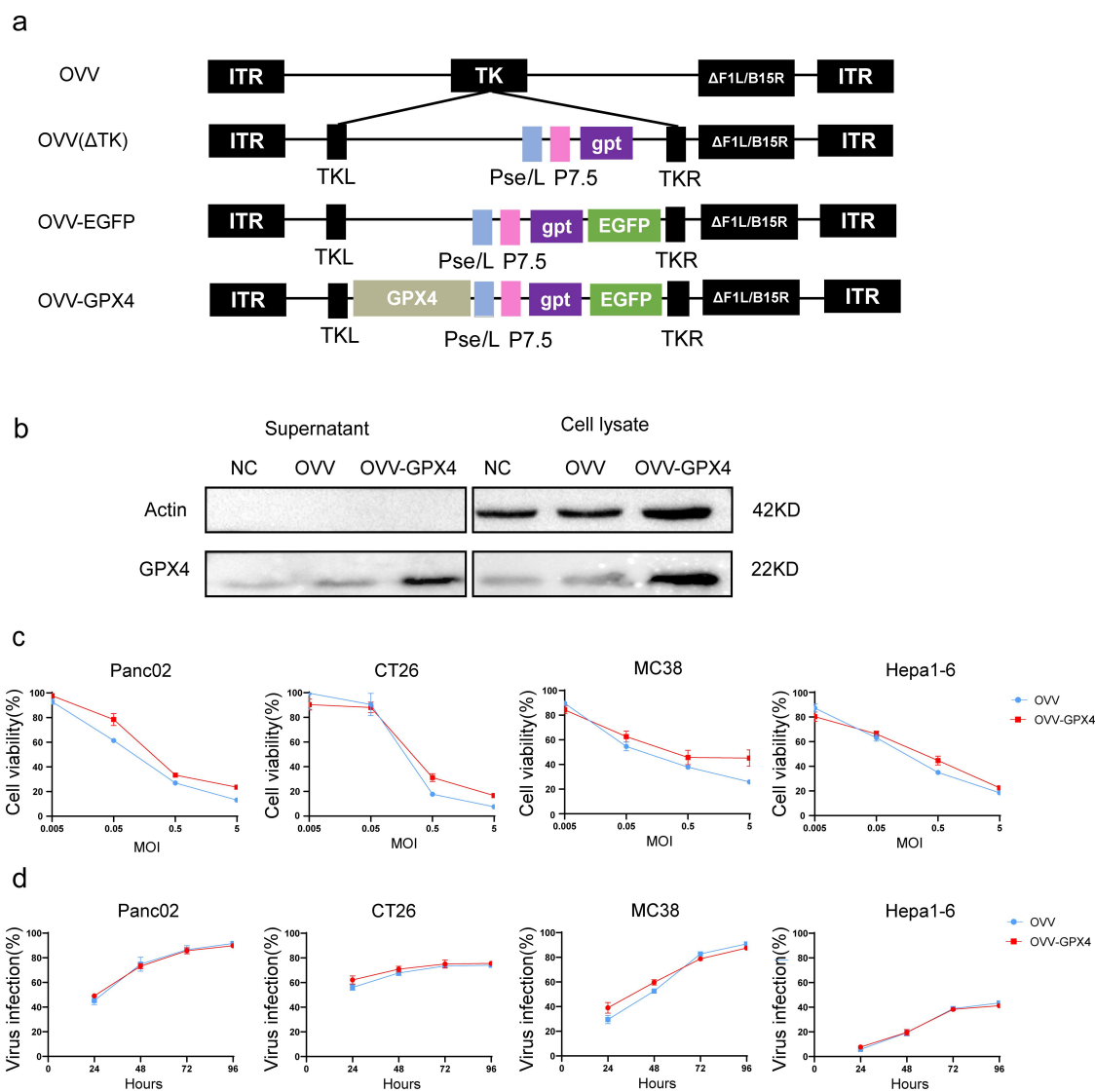


Figure 1. Generation of a GPX4-expressing oncolytic vaccinia virus and its oncolytic properties in vitro (a) Schematic representation of OVV-GPX4 structure. The GPX4 gene under the control of the promoter Pse/l was inserted into the TK gene of the vaccinia virus. TKR, right flank sequences of thymidine kinase gene; TKL, left flank sequences of thymidine kinase gene; gpt, guanine phosphoribosyl transferase; EGFP, enhanced green fluorescent protein; P7.5, vaccinia virus P7.5 early/late promoter; Pse/l, synthesized vaccinia virus early/late promoter. (b) Detection of GPX4 expression and secretion by western blot. Vero cells were infected with OVV or OVV-GPX4 at MOI 1. At 48 h post-infection, cell lysates and supernatants were collected, and GPX4 was detected with anti-GPX4 antibody. (c) Comparative cytotoxicity of OVV and OVV-GPX4. Panc02, CT26, MC38, and Hepa 1–6 cells infected with serial dilutions of OVV or OVV-GPX4. Cell viability was measured 48 h post-infection by CCK8. (d) Viral infectivity of OVV-GPX4. Panc02, CT26, MC38, and Hepa 1–6 cells infected with OVV or OVV-GPX4 at MOI of 0.1. At indicated time points, cells were harvested and detected by flow cytometry. Data represent the mean \pm standard deviation (SD) of \geq three independent experiments.

(Figure 2a,e). Additionally, we measured lipid peroxidation in these cells with a fluorescent Lipid probe (Bodipy 581/591 C11)⁴⁰ by flow cytometry (Figure 2a,f). OVV-GPX4 significantly reduced CD36 expression on CD8⁺ T cells, decreasing lipid accumulation and peroxidation.

OVV-GPX4 enhanced antitumor activity in vivo

After demonstrating that OVV-GPX4 affected T cells in vitro, we proceeded with a subcutaneous pancreatic cancer tumor model (Panc02) in C57BL/6 mice. The objective of this experiment was to assess the potential enhancement in the anti-tumor efficacy of OVV-GPX4. When the tumor volume of all mice was within the range of 50–100 mm³, it was considered as day 0. Refer to Figure 3a for the detailed injection scheme. Compared to other groups, the average tumor volume growth of the OVV-

GPX4 group was the smallest (Figure 3b). The OVV-GPX4 group had a significantly longer survival period (Figure 3c). The tumor growth curve for each mouse in Figure 3d showed that the OVV-GPX4 group had the slowest tumor growth. Simultaneously, we investigated the survival rate of CD8⁺ T cells in Panc02 model. The diagram was displayed in Figure S1a. Tumor tissues were collected from each group of mice on days 0, 2, 4, and 6, with day 0 being the first day after injection. The survival rate of CD8⁺ T cells was detected by flow cytometry indicating a time-dependent decrease in the survival rate of CD8⁺ T cells across all groups, but the OVV-GPX4 group maintained the highest level of survival rate (Figure S1b, c). The result suggested that OVV-GPX4 could enhance the survival rate of CD8⁺ T cells in Panc02 tumors.

Our experiments compared the distribution and abundance of OVV and OVV-GPX4 in tumor and normal tissue after

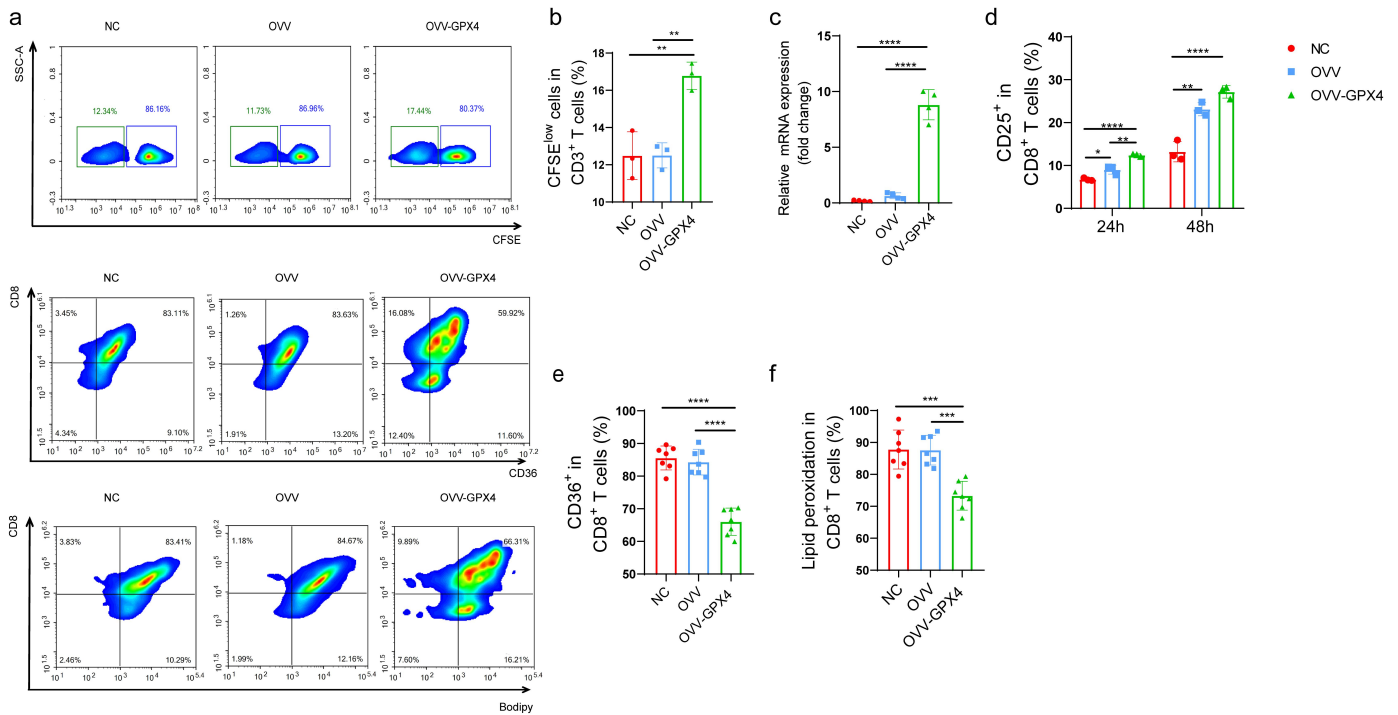


Figure 2. Effect of OVV-GPX4 on T cells in vitro (a) After staining T cells with CFSE and co-incubating them with tumor cells at a ratio of 6:1 (CD3⁺T: Panc02 cells), and adding OVV or OVV-GPX4 viral supernatant, T cell proliferation was measured by flow cytometry. In a parallel experiment, Co-culture of T cells with OVV or OVV-GPX4 (MOI = 10). After 48 h, the expression of CD36 and lipid peroxidation levels in CD8⁺T cells was evaluated by flow cytometry. (b) Representative diagram of flow cytometric analysis of T cell proliferation. (c) Bar chart showing expression of GPX4 in T cells. MOI for OVV or OVV-GPX4 infection of T cells was 10. Cells were collected 48 h after infection, RNA was extracted, and cDNA was reverse-transcribed. qPCR was utilized to detect GPX4 expression in cells. (d) Representative diagram of flow cytometric analysis of the activation indicator CD25 in CD8⁺ T cells. (e) Representative diagram of flow cytometric analysis of the expression of CD36 in CD8⁺ T cells. (f) Representative diagram of flow cytometric analysis of lipid peroxidation levels in CD8⁺ T cells. Data represent the mean \pm standard deviation (SD) of \geq three independent experiments. * $p < 0.05$; ** $p < 0.01$; *** $p < 0.001$; **** $p < 0.0001$.

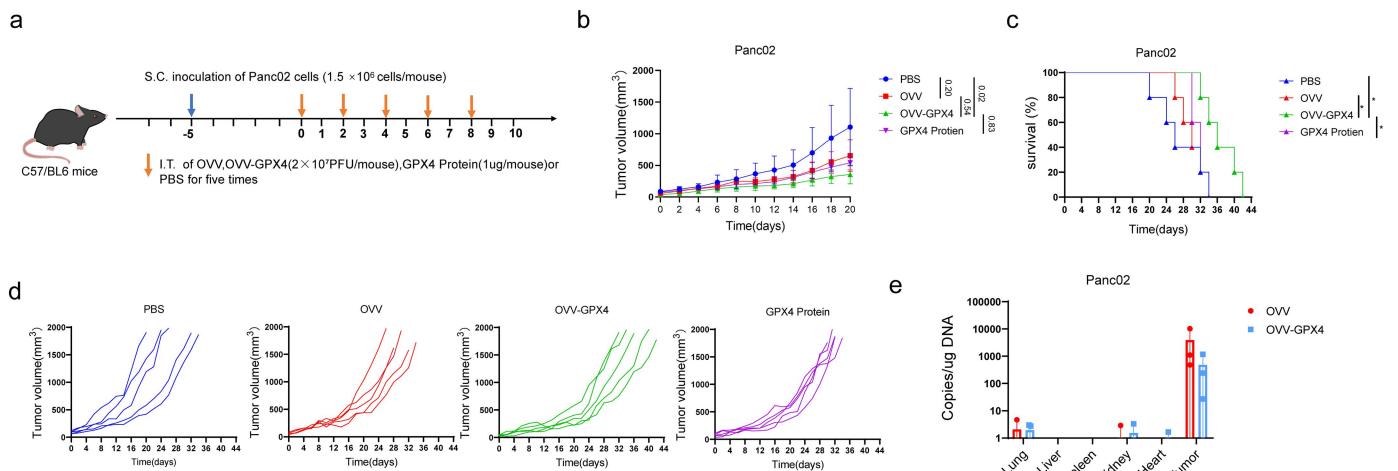


Figure 3. Intratumoral injection of OVV-GPX4 enhanced antitumor efficacy in subcutaneous Panc02 tumor models (a) C57BL/6 mice bearing subcutaneous Panc02 tumors were treated with PBS, OVV, OVV-GPX4 (2×10^7 pfu/tumor, I.T.), or GPX4 (1 μ g/tumor, I.T.) for five times. (b) Plot of mouse tumor progression. (c) Mouse survival curves. (d) Tumor growth curve for each mouse. (e) Bar chart showing the abundance of OVV and OVV-GPX4 in important organs and tumors of mice. Data represent the mean \pm standard deviation (SD) of \geq three independent experiments. * $p < 0.05$.

intratumoral injection. After tumor formation, we conducted animal experiments in which OVV and OVV-GPX4 were injected into the tumors every other day. After three times injections, their tumor tissues and vital organs, including the heart, liver, spleen, lung, and kidney, were extracted. In tumor tissue, viral DNA was detected by qPCR, which rarely accumulated in other organs. (Figure 3e).

Effect of OVV-GPX4 on the immune microenvironment and systemic immunity

To understand the enhanced anti-tumor efficacy of OVV-GPX4, Parallel tumor models were constructed to compare TME and spleen changes among different treatment groups. After establishing the Panc02 syngeneic model, tumors in mice were injected with PBS, OVV, OVV-GPX4, or GPX4 protein

for three times. After a two-day interval, the tumor and spleen tissue of the mice were processed into single-cell suspensions and the proportion of different immune cell populations was analyzed by flow cytometry analysis. The OVV-GPX4 group could more significantly increase the proportion of CD8⁺T cells in TME than the PBS and GPX4 protein groups (Figure 4a,b) and the expression of ki67 was significantly higher than others (Figure 4a,c). In the spleen, the OVV-GPX4 group had a higher ratio of CD8⁺T cells to CD3⁺T cells than PBS, OVV and GPX4 protein groups (Figure 5a,b) and higher ki67 expression in CD8⁺ T cells (Figure 5a,c). Meanwhile, compared with the spleen, we could see changes in the subtypes of T cells in TME, with a significant increase in the proportion of CD8⁺T cells. These evidences indicated that the OVV-GPX4 group were more capable of recruiting CD8⁺T cells with primary tumor-killing effects and promoting their proliferation. OVV and OVV-GPX4 treatment also reduced MDSC cells in the TME and spleen (Figures 4a,d 5a, d), indicating less immunosuppressive cell infiltration, but this phenomenon is more significant in the OVV-GPX4 group. To confirm T cells producing more cytokines in response to cytotoxicity, our subsequent experiments demonstrated heightened levels of CD8⁺ T cells secreting IFN- γ in the OVV-GPX4 group's tumors and spleens compared with PBS and OVV group. The average levels of CD8⁺ T cells secreting IFN- γ in the spleen was higher than that in the tumor in OVV-GPX4, it indicated that the function of CD8⁺T was inhibited in TME (Figures 4e, 5e). However, there was not outstanding difference in the ability of CD8⁺T cells to secrete IFN- γ between OVV-GPX4 and GPX4 protein group in spleens (Figure 5e). In the OVV-GPX4 group, the levels of CD8⁺ T cells producing perforin-1 were significantly different from the PBS group in spleens (Figure 5f), but this phenomenon lacks significance in tumors (Figure 4f). The TIM-3 marker on the surface of T cells in OVV-GPX4 group noticeable declined compared to PBS and GPX4 protein groups (Figure 4h). We also detected that LAG-3 marker decreased on the surface of T cells in the OVV-GPX4 group than others (Figure 4i), but the expression of PD-1 was remarkable higher than PBS and GPX4 protein groups (Figure 4a,g). Lastly, OVV-GPX4 diminished Foxp3⁺ CD4⁺T Treg infiltration in tumors than PBS (Figure 4j). This series of findings indicated that OVV-GPX4 could enhance the proliferative abilities of T cells, reverse their depleted state, exert a strong effector capacity, and improve the immune-suppressive microenvironment.

Similar to the aforementioned outcomes, CD8⁺T cell infiltration was also examined in paraffin slices of mouse tumors from each group by IHC in a parallel experiment. The OVV-GPX4 group exhibited a greater abundance of brown marker staining in comparison to the other groups (Figure 4k).

To evaluate whether local injection of OVV-GPX4 could induce an abscopal effect, we used a bilateral Panc02 tumor model (Figure S2a). Although both OVV and OVV-GPX4 exhibited therapeutic effects on primary and distant tumors, OVV-GPX4 distinguished itself from PBS in more substantial differences when compared to OVV (Figure S2b). The findings indicated that the therapeutic efficacy of OVV-GPX4 extended beyond local regions and impacted systemic immunity.

CD8⁺ T cells mediated the antitumor immunity of OVV-GPX4

To reveal the role of CD8⁺ T and CD4⁺ T cells in mediating the antitumor activity of OVV-GPX4, we depleted these two types of lymphocytes and analyzed whether their depletion would affect the antitumor efficacy of OVV-GPX4 in the Panc02 subcutaneous syngeneic model. Initially, we verified the blocking effect of anti-CD8 and anti-CD4 monoclonal antibodies. As expected, the CD8⁺ T and CD4⁺ T cells in tumors were completely depleted after the injection of the corresponding monoclonal antibody (Figure 6a,b). Following the successful inhibition of the function of CD8⁺ T and CD4⁺ T cells, we continuously monitored the tumor volume of mice in each group (Figure 6c). Consistent with previous results, treatment of mice with OVV-GPX4 significantly decreased the tumor volume. Conversely, the depletion of CD8⁺ T cells resulted in the reversal of tumor volume reduction (Figure 6d,e). These results indicated that the depletion of CD8⁺ T cells partially abrogated the antitumor efficacy of OVV-GPX4, while the depletion of CD4⁺ cells had no obvious impact. CD8⁺ T cell is a major immune cell type that mediates the antitumor immunity of OVV-GPX4.

OVV-GPX4 therapy in conjunction with immune checkpoint inhibitors

The OVV-GPX4 group had higher PD-1 levels on CD8⁺T cells in the Panc02 syngeneic model (Figure 4a,g), suggesting that ICB may boost immune response and antitumor effects. Mice with tumor volumes between 50 and 100 mm³ were randomly assigned to groups and injected with PBS or OVV-GPX4 alone or in combination with an anti-PD-1 antibody (Figure 7a). Next, tumor volume was measured. On day 22, the OVV-GPX4 and anti-PD-1 antibody combination treatment group had an average tumor volume of 327.342 mm³, while the PBS and anti-PD-1 antibody-only groups had 1263.02 and 907.07 mm³, respectively (Figure 7b). We plotted the survival curves of mice and found that the combined group survived longer than the others (Figure 7c). Individual tumor growth curves indicated that combination therapy significantly slowed tumor growth without causing regression (Figure 7d).

Immune mediation mechanism for OVV-GPX4

Targeted transcriptome analysis helped us to understand signal pathways and immune-mediating mechanisms of OVV-GPX4. After establishing the Panc02 syngeneic model, tumors were injected with PBS, OVV, or OVV-GPX4 and subsequently underwent RNA sequencing. The research findings suggested that the OVV-GPX4 group exhibited the most pronounced differences in genes associated with chemokine signaling pathways compared to the PBS and OVV groups. The maximum number of differentially expressed genes were in the cytokine-cytokine receptor interaction pathways (Figure 8a). The thermographic representation in Figure 8b,c shows the differential genes in the chemokine signaling pathway and cytokine-cytokine receptor interaction pathway. Genes for the C-type lectin receptor signaling pathway, leukocyte transendothelial

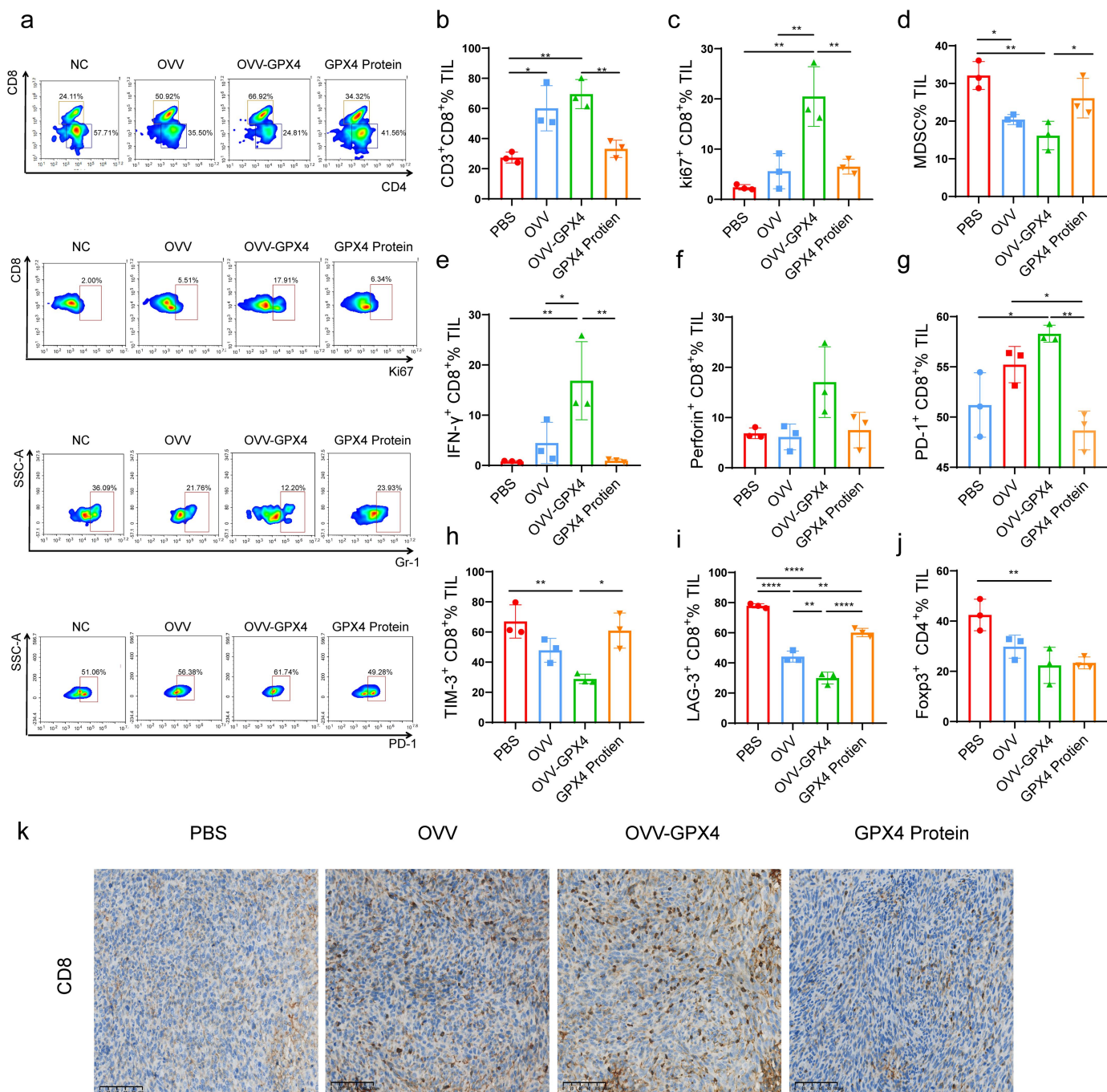


Figure 4. Intratumoral injection of OVV-GPX4 improved immune microenvironment in Panc02 tumor model (a) C57BL/6 mice bearing subcutaneous Panc02 tumors were treated with PBS, OVV, OVV-GPX4 (2×10^7 pfu/tumor, I.T.), or GPX4 (1 μ g/tumor, I.T.). On day 2 after virus injection, tumors were harvested, and a cell suspension was prepared. Percentages of CD8⁺T cells were analyzed by flow cytometry. In other parallel experiments, CD8⁺T cell proliferation indicator Ki67, percentages of MDSCs and the expression of PD-1 on the surface of CD8⁺T cells in tumors was analyzed by flow cytometry. (b) Representative diagram of flow cytometric analysis of CD8⁺T cell proliferation indicator Ki67 in tumors. (c) Representative diagram of flow cytometric analysis showing percentages of MDSCs in tumors. (d) Representative diagram of flow cytometric analysis showing percentages of MDSCs in tumors. (e) Representative diagram of flow cytometric analysis of IFN- γ producing in CD8⁺T cells, which exert effector functions in tumors. (f) Representative diagram of flow cytometric analysis of producing perforin-1 in CD8⁺T cell in tumors. (g) Representative diagram of flow cytometric analysis of PD-1 on the surface of CD8⁺T cells in tumors. (h,i) Representative diagram of flow cytometric analysis of depletion indexes tim-3 and LAG-3 on the surface of CD8⁺T cell in tumors. (j) Representative diagram of flow cytometric analysis of percentage of Foxp3⁺ CD4⁺ Treg cells in tumors. (k) Detection of CD8⁺T infiltration in tumors by immunohistochemistry. Scale bar, 100 μ m. ($n = 3$ per group). Data represent the mean \pm standard deviation (SD) of three independent experiments. * $p < 0.05$; ** $p < 0.01$; *** $p < 0.0001$.

migration, and other innate immune system signaling pathways were also enriched (Figure 8a). After that, we used qPCR to confirm that the OVV-GPX4 experimental group had increased levels of chemokines like CCL4, CXCL9, CXCL10,

and CXCL13. Moreover, there were notable differences in the expression of surface co-stimulatory molecules, specifically CD28 and ICOS, as well as the cytokine granzyme B (GZMB) (Figure 8d).

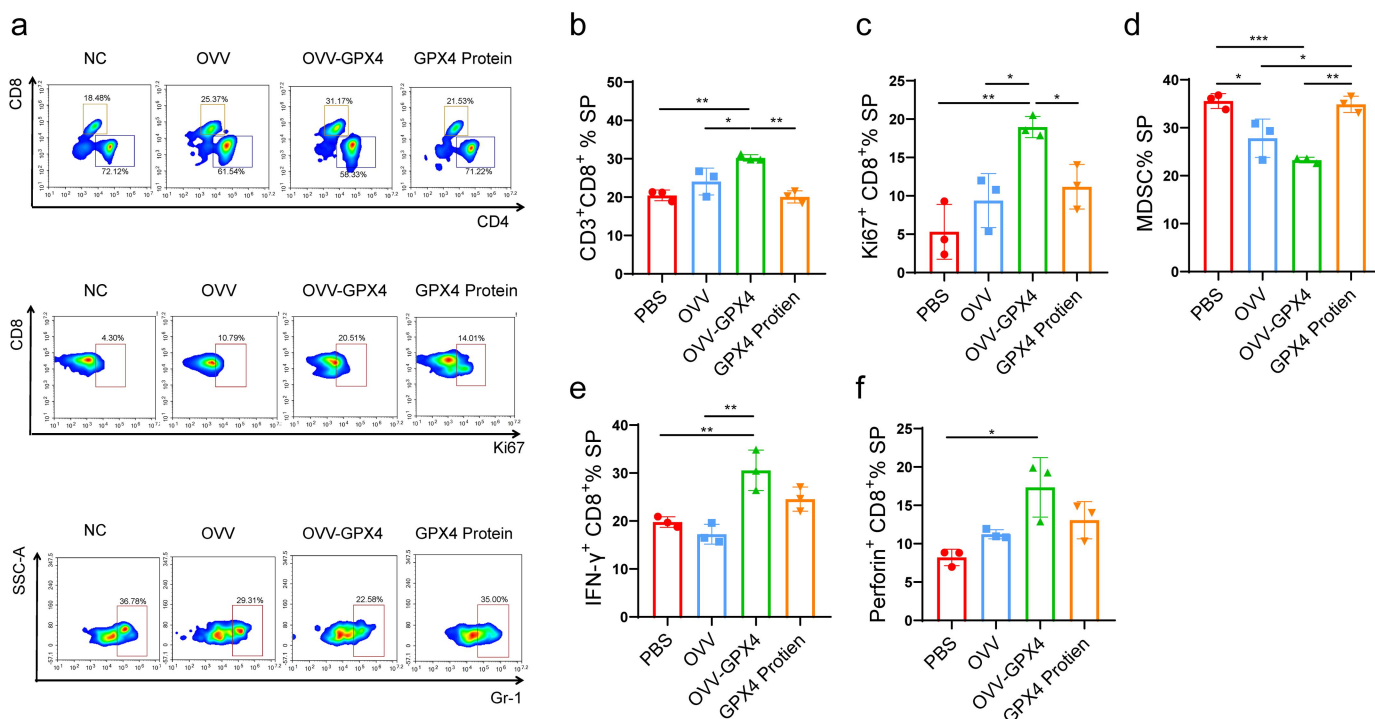


Figure 5. Intratumoral injection of OVV-GPX4 improved systemic immunity in Panc02 tumor model (a) C57BL/6 mice bearing subcutaneous Panc02 tumors were treated with PBS, OVV, OVV-GPX4 (2×10^7 pfu/tumor, I.T.), or GPX4 (1 μ g/tumor, I.T.). On day 2 after virus injection, spleens were harvested, and a cell suspension was prepared. Percentages of CD8⁺T cells, proliferation indicator Ki67 and percentages of MDSCs in spleens were analyzed by flow cytometry. (b) Representative diagram of flow cytometric analysis of percentages of CD8⁺T cells in spleens. (c) Representative diagram of flow cytometric analysis of CD8⁺T cell proliferation indicator Ki67 in spleens. (d) Representative diagram of flow cytometric analysis showing percentages of MDSCs in spleens. (e) Representative diagram of flow cytometric analysis of IFN- γ producing in CD8⁺T cells in spleens. (f) Representative diagram of flow cytometric analysis of perforin-1 producing in CD8⁺T cells in spleens. Data represent the mean \pm standard deviation (SD) of three independent experiments. * $p < 0.05$; ** $p < 0.01$; *** $p < 0.001$.

Discussion

Solid tumor immunotherapies have gained popularity in recent years. However, insufficient CTLs, IFN- γ activation markers, and low GZMB expression in the tumor core have limited the efficacy of these therapies.^{5,6} Only a small percentage of patients with high TIL counts benefit from ICB monotherapy. Thus, OVVs are promising immunotherapies because they can mobilize immune cells to reenter the tumor in the PDAC microenvironment. The vaccinia virus was chosen as the payload for this experiment due to its ability to express recombinant genes, facilitated by its large genome to insert exogenous genes up to 40kd.⁴¹ Meanwhile, the OVV has an efficient life cycle and can generate virus offspring in just 6 hours. The OVV replicated within the host cytoplasm without integrating into DNA, combined with its history as a smallpox vaccine, ensures its safety.¹² We deleted the TK gene and added GPX4 in OVV, which didn't affect its ability to infect and kill tumor cells. Further proof also showed that the virus could increase the expression of GPX4 in T cells. OVVs have the potential to serve as an in situ cancer vaccine because they induce highly immunogenic cell death, resulting in the release of tumor-associated antigens, danger-associated molecular patterns and pathogen-associated molecular patterns. However, if the activation of this antiviral immune response is excessively potent, which can lead to rapid virus clearance, thereby limiting the induction of antitumor responses.⁴² Hence, it is crucial to find the optimal balance between antiviral immune response and antitumor

immune response. Our limitation was the lack of real-time measurement of the virus titers and antiviral antibodies. In future research, we will compare the virus titers and antiviral antibodies generated through various injection techniques and dosages. The objective is to attain a prolonged viral infection and reduce the levels of neutralizing antibodies, thereby optimizing the anti-tumor efficacy. Currently, many strategies have also emerged to extend the half-life of proteins to achieve better therapeutic effects, including sequential modification, attachment of fatty acids to peptides,⁴³ improving the affinity of the neonatal Fc receptor,⁴⁴ and so on. These strategies suggest that monitoring and increasing the half-life of GPX4 combined with OVV may have more significant therapeutic effects on tumors, and we will conduct research in the future.

GPX4 assumes a crucial function in safeguarding cells against the detrimental effects of lipid peroxidation. Studies have shown that the ferroptosis-inducer erastin and RSL3((1S,3 R)-RSL3) derivatives inhibit the growth of tumor cells by consuming glutathione and by binding to and inactivating GPX4 in xenotransplantation model mice, respectively.²⁸ Despite that cancer cells avoid ferroptosis by activating antioxidant signaling pathways, such as the SLC7A11/GPX4 axis,⁴⁵ T cells were found to undergo metabolic challenges in TME, and GPX4 inhibitor compounds were more toxic to CD8⁺T cells than tumor cells.³¹ Furthermore, the deficiency of GPX4 in T cell significantly compromises the peripheral bloodstream CD8⁺T cell effector function and homeostasis.⁴⁶ According to some studies,

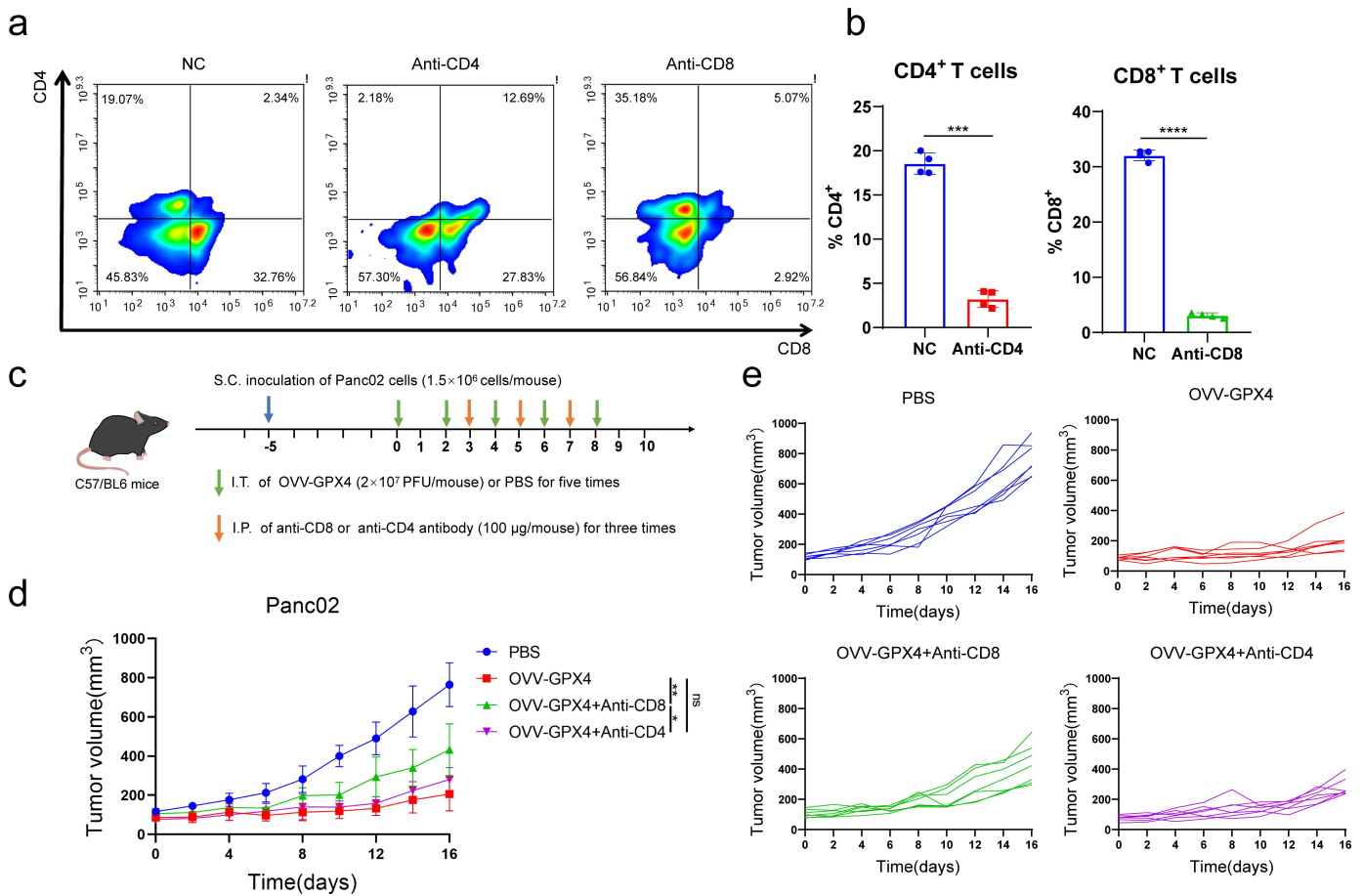


Figure 6. CD8⁺ T cells mediated the antitumor immunity of OVV-GPX4 (a) The depletion of CD8⁺ T and CD4⁺ T cells in the tumor of mice was analyzed by flow cytometry. (b) Flow cytometric analysis of the proportion of CD8⁺ T cells and CD4⁺ T cells. (c) Treatment scheme of Panc02 S.C. tumor models. C57BL/6 mice bearing subcutaneous Panc02 tumors were injected with PBS, OVV-GPX4 (2×10^7 pfu/mouse, I.T.), OVV-GPX4 (2×10^7 pfu/mouse, I.T.) combined with anti-CD4 or anti-CD8 antibody (100 μ g/mouse, I.P.). Tumor volume was measured every 2 days. (d) Plot of mouse tumor progression. (e) Individual tumor growth curve. Data represent the mean \pm standard deviation (SD) of \geq three independent experiments. ns > 0.05; * p < 0.05; ** p < 0.01; *** p < 0.001; **** p < 0.0001.

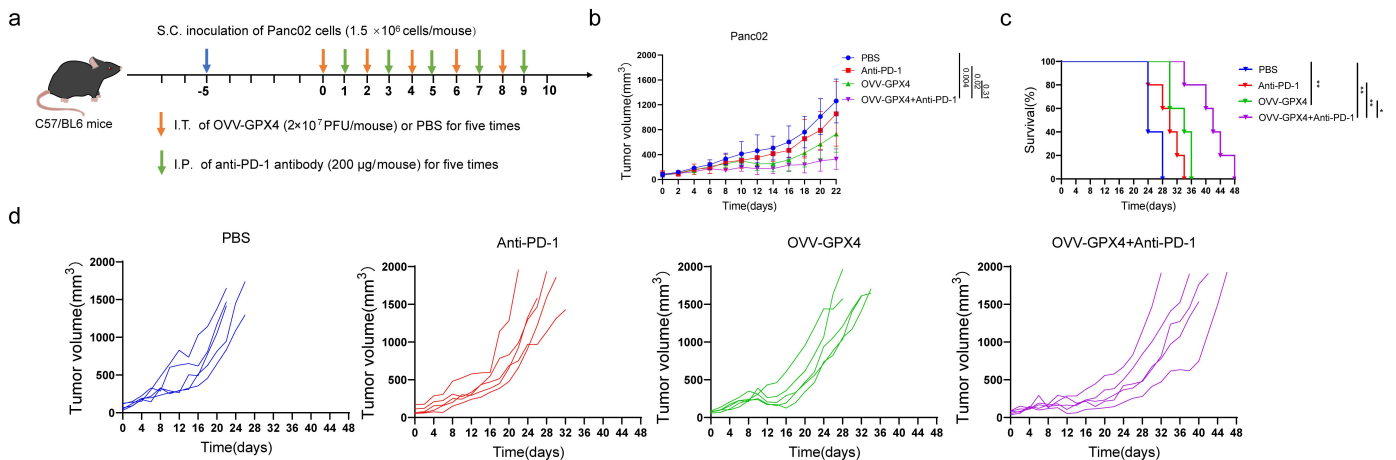


Figure 7. Intratumoral injection of OVV-GPX4 combined with anti-PD-1 antibody enhanced antitumor efficacy in subcutaneous Panc02 tumor model (a) Illustration of mouse injection procedure. C57BL/6 mice bearing subcutaneous Panc02 tumors were injected with PBS, OVV-GPX4 (2×10^7 pfu/mouse, I.T.), anti-PD-1 antibody (200 μ g/mouse, I.P.), or OVV-GPX4 combined with anti-PD-1 antibody for five times. Tumor volume was measured every 2 days. (b) Plot of mouse tumor progression. (c) Mouse survival curves. (d) Tumor growth curve for each mouse. Data represent the mean \pm standard deviation (SD) of five independent experiments. * p < 0.05; ** p < 0.01.

CD8⁺ T cells underwent CD36-mediated excessive uptake of fatty acids and GPX4 inhibitors, leading to ferroptosis and tumor immune evasion.³⁷ In contrast, T cells transduced with a retrovirus overexpressing GPX4 showed reduced levels of lipid

peroxidation, alleviated depletion, and a stronger antitumor effect.³⁸ Similar results have been confirmed by our experiments, both CD36 expression on the surface of mouse peripheral blood T lymphocytes and lipid peroxidation decreased after co-

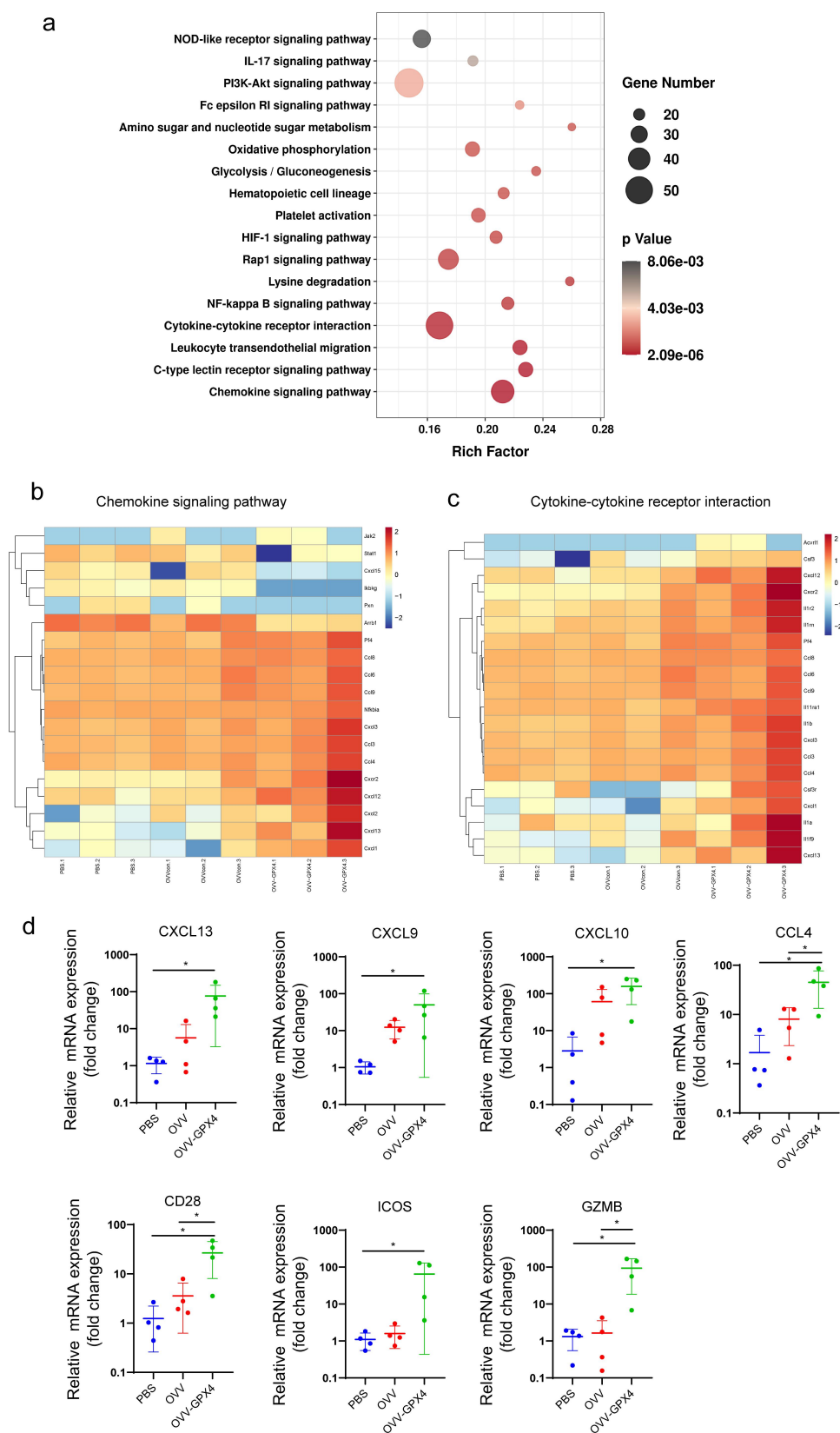


Figure 8. Immune mediation mechanism of OVV-GPX4 (a) C57BL/6 mice bearing subcutaneous Panc02 tumors were treated with PBS, OVV, or OVV-GPX4 (2×10^7 pfu/tumor, I.T.) for three times. On day 2 after virus injection, RNA from fresh tumor tissues was sequenced. Bubble plot of KEGG analysis of signaling pathway gene expression enrichment. (b) Heat map of differentially expressed genes in the chemokine signaling pathway. (c) Heat map of differentially expressed genes in the cytokine-cytokine receptor interaction pathways. (d) Detection of fold changes in CCL4, CXCL9, CXCL10, CXCL13, ICOS, CD28, and GZMB at mRNA level by qPCR. Data represent the mean \pm standard deviation (SD) of \geq three independent experiments. * $p < 0.05$.

incubation with the OVV-GPX4 supernatant. In addition, the ability of proliferation and the proportion of CD25⁺-activated T cells increased significantly in the group treated with OVV-GPX4. In constructed Panc02 tumor models, OVV-GPX4 prolonged the survival rate of CD8⁺T in tumors and played an important role in improving the immune microenvironment and systemic immunity.

GPX4 has the effect of promoting CD8⁺T, which plays an anti-tumor role. Still, some studies have found that Treg-specific GPX4 deletion increases mitochondrial superoxide, TH17 response IL-1b, tumor growth inhibition, and anti-tumor immunity⁴⁷ Likewise, it has been reported that GPX4 protects the follicular T helper cells that protect the germinal center reaction from ferroptosis and promote antibody responses.⁴⁸ GPX4 not only increases the effectiveness of CD8⁺T cells but also promotes the development of immunosuppressive Treg cells. To investigate the comprehensive effect of OVV-GPX4 in TME, we employed the Panc02 mouse model and discovered that OVV-GPX4 significantly inhibited tumor growth compared to the other treatments. Subsequently, we designed a CD8⁺T and CD4⁺T depletion experiment to investigate which immune cell type is primarily responsible for antitumor activity. The results indicated that CD8⁺ T is the main type of immune cell rather than CD4⁺ T for anti-tumor therapy.

Talimogene laherparepvec (T-VEC) is a herpes simplex type 1 virus modified with a granulocyte-macrophage colony-stimulating gene (GM-CSF). Compared to the use of ipilimumab only to block cytotoxic T cell-associated antigen 4 (CTLA-4), a combination of ipilimumab and T-VEC induced a stronger immune response in a phase 2 randomized trial of advanced melanoma⁴⁹ T-VEC also attained an objective response rate of 62% and a complete response rate of 33%⁵⁰ when combined with the anti-PD-1 antibody pembrolizumab in a phase 1b trial of advanced melanoma treatments. Here, we demonstrated that GPX4-loaded OVV changed the immune state of the PDAC microenvironment and increased PD-1 expression on CD8⁺T cells. Combining OVV-GPX4 and anti-PD-1 monoclonal antibodies increased the survival of tumor-bearing mice. However, the combined effect of anti-PD-1 monoclonal antibody was also moderate, indicating other factors hindering anti-tumor effects. We will probe into other elements that contribute to tumor escape in the future.

An investigation of the immune-mediated mechanisms showed that the difference in gene expressions was most significant in the chemokine signal pathway in the OVV-GPX4 group, while the cytokine and cytokine receptor pathways were highlighted as having the most differentially expressed genes involved. However, in this study, we did not construct the GPX4 protein group, which is a limitation of our study. In our next initiatives, we will investigate the immune-mediated mechanisms of GPX4 protein group, increase the sample size, and gain a more comprehensive understanding of the TME.

In conclusion, our research results demonstrated the immunotherapeutic potential of OVV-GPX4. As an agent for oncolytic virotherapy, it can improve the TME, regulate the status of effector T cells, and exert a stronger anti-tumor effect. In addition, it can be synergistically combined with ICB therapies to overcome the limitations of a single-drug therapy, and based

on our data, human studies in patients with PDAC may be warranted.

Disclosure statement

No potential conflict of interest was reported by the author(s).

Funding

This study was supported by the Foundation of Science Technology Department of Zhejiang Province [No. LGF22H080012, No. LGF22H080008], Zhejiang Provincial Medical Technology Plan Project [No. 2022KY505, No. 2020KY052].

Author contributions

WW and LT analyzed data, performed experiments, drew figures and tables, and wrote the manuscript. GZ and SW funded this study, while XZ, LZ, HD, and GZ conducted experiments and statistical analysis. XT, SW, and YC designed the study, assisted with logistics, and reviewed paper drafts. Each author approved the final manuscript after this review.

Data availability statement

The results/data/figures in this manuscript have not been published elsewhere, nor are they under consideration by another publisher.

References

1. Siegel RL, Miller KD, Wagle NS, Jemal A. Cancer statistics, 2023. *CA Cancer J Clin.* 2023;73(1):17–48. doi:10.3322/caac.21763.
2. Wood LD, Canto MI, Jaffee EM, Simeone DM. Pancreatic cancer: pathogenesis, screening, diagnosis, and treatment. *Gastroenterology.* 2022;163(2):386–402 e381. doi:10.1053/j.gastro.2022.03.056.
3. Farren MR, Sayegh L, Ware MB, Chen H-R, Gong J, Liang Y, Krasinskas A, Maithel SK, Zaidi M, Sarmiento JM, et al. Immunologic alterations in the pancreatic cancer microenvironment of patients treated with neoadjuvant chemotherapy and radiotherapy. *JCI Insight.* 2020;5(1):Insight 5: 2020. doi: 10.1172/jci.insight.130362.
4. Halbrook CJ, Lyssiotis CA, Pasca di Magliano M, Maitra A. Pasca di Magliano M and Maitra A: pancreatic cancer: advances and challenges. *Cell.* 2023;186(8):1729–1754. doi:10.1016/j.cell.2023.02.014.
5. Binnewies M, Roberts EW, Kersten K, Chan V, Fearon DF, Merad M, Coussens LM, Gabrilovich DI, Ostrand-Rosenberg S, Hedrick CC, et al. Understanding the tumor immune microenvironment (TIME) for effective therapy. *Nat Med.* 2018;24(5):541–550. doi:10.1038/s41591-018-0014-x.
6. Fan JQ, Wang MF, Chen HL, Shang D, Das JK, Song J. Current advances and outlooks in immunotherapy for pancreatic ductal adenocarcinoma. *Mol Cancer.* 2020;19(1):32. doi:10.1186/s12943-020-01151-3.
7. Brahmer JR, Tykodi SS, Chow LQ, Hwu W-J, Topalian SL, Hwu P, Drake CG, Camacho LH, Kauh J, Odunsi K, et al. Safety and activity of anti-PD-L1 antibody in patients with advanced cancer. *N Engl J Med.* 2012;366(26):2455–2465. doi:10.1056/NEJMoa1200694.
8. Ribas A, Wolchok JD. Cancer immunotherapy using checkpoint blockade. *Science.* 2018;359(6382):1350–1355. doi:10.1126/science.aar4060.
9. Bear AS, Vonderheide RH, O'Hara MH. Challenges and opportunities for pancreatic cancer immunotherapy. *Cancer Cell.* 2020;38(6):788–802. doi:10.1016/j.ccell.2020.08.004.

10. Lawler SE, Speranza MC, Cho CF, Chiocca EA. Oncolytic viruses in cancer treatment: a review. *JAMA Oncol.* 2017;3(6):841–849. doi:10.1001/jamaoncol.2016.2064.
11. Tian Y, Xie D, Yang L. Engineering strategies to enhance oncolytic viruses in cancer immunotherapy. *Signal Transduct Target Ther.* 2022;7(1):117. doi:10.1038/s41392-022-00951-x.
12. Guo ZS, Lu B, Guo Z, Giehl E, Feist M, Dai E, Liu W, Storkus WJ, He Y, Liu Z, et al. Vaccinia virus-mediated cancer immunotherapy: cancer vaccines and oncolytics. *J Immunother Cancer.* 2019;7(1):6. doi:10.1186/s40425-018-0495-7.
13. Kaufman HL, Deraffle G, Mitcham J, Moroziewicz D, Cohen S, M, Hurst-Wicker K.S., Cheung K., Lee D.S., Divito J., Voulo M., Donovan J, et al. Targeting the local tumor microenvironment with vaccinia virus expressing B7.1 for the treatment of melanoma. *J Clin Invest.* 2005;115(7):1903–1912. doi:10.1172/JCI24624.
14. Eriksson E, Milenova I, Wenthe J, Stähle M, Leja-Jarblad J, Ullenhag G, Dimberg A, Moreno R, Alemany R, Loskog A, et al. Shaping the tumor stroma and sparking immune activation by CD40 and 4-1BB signaling induced by an armed oncolytic virus. *Clin Cancer Res.* 2017;23(19):5846–5857. doi:10.1158/1078-0432.CCR-17-0285.
15. Robinson M, Li B, Ge Y, Ko D, Yendluri S, Harding T, VanRoey M, Spindler KR, Jooss K. Novel immunocompetent murine tumor model for evaluation of conditionally replication-competent (oncolytic) murine adenoviral vectors. *J Virol.* 2009;83(8):3450–3462. doi:10.1128/JVI.02561-08.
16. Li J, O'Malley M, Urban J, Sampath P, Guo ZS, Kalinski P, Thorne SH, Bartlett DL. Chemokine expression from oncolytic vaccinia virus enhances vaccine therapies of cancer. *Mol Ther.* 2011;19(4):650–657. doi:10.1038/mt.2010.312.
17. Li F, Sheng Y, Hou W, Sampath P, Byrd D, Thorne S, Zhang Y. CCL5-armed oncolytic virus augments CCR5-engineered NK cell infiltration and antitumor efficiency. *J Immunother Cancer.* 2020;8(1):e000131. doi:10.1136/jitc-2019-000131.
18. Shinsuke Nakao YA, Tasaki M, Yamashita M, Murakami R, Tatsuya Kawase NA, Nakatake M, Kurosaki H, Mori M, Takeuchi M, Mori M. Takafumi Nakamura: intratumoral expression of IL-7 and IL-12 using an oncolytic virus increases systemic sensitivity to immune checkpoint blockade. *Sci Transl Med.* 2020;12(526):eaax7992. doi:10.1126/scitranslmed.aax7992.
19. Pearl TM, Markert JM, Cassady KA, Ghonime MG. Oncolytic virus-based cytokine expression to improve immune activity in brain and solid tumors. *Mol Ther Oncolytics.* 2019;13:14–21. doi:10.1016/j.omto.2019.03.001.
20. Barber S, Barber GN. Oncolytic viruses as antigen agnostic tumor vaccines. *Cancer Cell.* 2018;33(4):599–605. doi:10.1016/j.ccell.2018.03.011.
21. Tian C, Liu J, Zhou H, Li J, Sun C, Zhu W, Yin Y, Li X. Enhanced anti-tumor response elicited by a novel oncolytic HSV-1 engineered with an anti-PD-1 antibody. *Cancer Lett.* 2021;518:49–58. doi:10.1016/j.canlet.2021.06.005.
22. Lei GL, Wang LP, Dong SH, Sun F, Cheng J-X, Yang X-L, Zhang S-G, Wang X-L, Wang X-X, Yang P-H, et al. A recombinant influenza virus with a CTLA4-specific scFv inhibits tumor growth in a mouse model. *Cell Biol Int.* 2021;45(6):1202–1210. doi:10.1002/cbin.11559.
23. Qiao J, Kottke T, Willmon C, Galivo F, Wongthida P, Diaz RM, Thompson J, Ryno P, Barber GN, Chester J, et al. Purging metastases in lymphoid organs using a combination of antigen-nonspecific adoptive T cell therapy, oncolytic virotherapy and immunotherapy. *Nat Med.* 2008;14(1):37–44. doi:10.1038/nm1681.
24. Willmon C, Harrington K, Kottke T, Prestwich R, Melcher A, Vile R. Cell carriers for oncolytic viruses: fed ex for cancer therapy. *Mol Ther.* 2009;17(10):1667–1676. doi:10.1038/mt.2009.194.
25. Zheng N, Fang J, Xue G, Wang Z, Li X, Zhou M, Jin G, Rahman MM, McFadden G, Lu Y, et al. Induction of tumor cell autolysis by myxoma virus-infected CAR-T and TCR-T cells to overcome primary and acquired resistance. *Cancer Cell.* 2022;40(9):973–985 e977. doi:10.1016/j.ccell.2022.08.001.
26. Iankov ID, Blechacz B, Liu C, Schmeckpeper JD, Tarara JE, Federspiel MJ, Caplice N, Russell SJ. Infected cell carriers: a new strategy for systemic delivery of oncolytic measles viruses in cancer virotherapy. *Mol Ther.* 2007;15(1):114–122. doi:10.1038/sj.mt.6300020.
27. Yu F, Wang X, Guo ZS, Bartlett DL, Gottschalk SM, Song XT. T-cell engager-armed oncolytic vaccinia virus significantly enhances antitumor therapy. *Mol Ther.* 2014;22(1):102–111. doi:10.1038/mt.2013.240.
28. Yang WS, SriRamaratnam R, Welsch ME, Shimada K, Skouta R, Viswanathan V, Cheah J, Clemons P, Shamji A, Clish C, et al. Regulation of ferroptotic cancer cell death by GPX4. *Cell.* 2014;156(1–2):317–331. doi:10.1016/j.cell.2013.12.010.
29. Zou Y, Palte MJ, Deik AA, Li H, Eaton JK, Wang W, Tseng Y-Y, Deasy R, Kost-Alimova M, Dančik V, et al. A GPX4-dependent cancer cell state underlies the clear-cell morphology and confers sensitivity to ferroptosis. *Nat Commun.* 2019;10(1):2019. doi:10.1038/s41467-019-09277-9.
30. Eaton JF, Ruberto RA, Moosmayer D, Hilpmann A, Ryan MJ, Zimmermann K, Cai LL, Niehues M, Badock V, Kramm A, et al. Selective covalent targeting of GPX4 using masked nitrile-oxide electrophiles. *Nat Chem Biol.* 2020;5(5):497–506. doi:10.1038/s41589-020-0501-5.
31. Drijvers JM, Gillis JE, Muijlwijk T, Nguyen TH, Gaudio EF, Harris IS, LaFleur MW, Ringel AE, Yao C-H, Kurmi K, et al. Pharmacologic screening identifies metabolic vulnerabilities of CD8(+) T cells. *Cancer Immunol Res.* 2021;9(2):184–199. doi:10.1158/2326-6066.CIR-20-0384.
32. Yang K, Wang X, Song C, He Z, Wang R, Xu Y, Jiang G, Wan Y, Mei J, Mao W, et al. The role of lipid metabolic reprogramming in tumor microenvironment. *Theranostics.* 2023;13(6):1774–1808. doi:10.7150/thno.82920.
33. Gubser PM, Bantug GR, Razik L, Fischer M, Dimeloe S, Hoenger G, Durovic B, Jauch A, Hess C. Rapid effector function of memory CD8+ T cells requires an immediate-early glycolytic switch. *Nat Immunol.* 2013;14(10):1064–1072. doi:10.1038/ni.2687.
34. Yu W, Lei Q, Yang L, Qin G, Liu S, Wang D, Ping Y, Zhang Y. Contradictory roles of lipid metabolism in immune response within the tumor microenvironment. *J Hematol Oncol.* 2021;14(1):187. doi:10.1186/s13045-021-01200-4.
35. Ingold I, Berndt C, Schmitt S, Doll S, Poschmann G, Buday K, Roveri A, Peng X, Porto Freitas F, Seibt T, et al. Selenium utilization by GPX4 is required to prevent hydroperoxide-induced ferroptosis. *Cell.* 2018;172(3):409–422 e421. doi:10.1016/j.cell.2017.11.048.
36. Li Y, Huang X, Yang G, Xu K, Yin Y, Brecchia G, Yin J. CD36 favours fat sensing and transport to govern lipid metabolism. *Prog Lipid Res.* 2022;88:101193. doi:10.1016/j.plipres.2022.101193.
37. Ma X, Xiao L, Liu L, Ye L, Su P, Bi E, Wang Q, Yang M, Qian J, Yi Q, et al. CD36-mediated ferroptosis dampens intratumoral CD8+ T cell effector function and impairs their antitumor ability. *Cell Metab.* 2021;33(5):1001–1012.e5. doi:10.1016/j.cmet.2021.02.015.
38. Xu S, Chaudhary O, Rodriguez-Morales P, Sun X, Chen D, Zappasodi R, Xu Z, Pinto AFM, Williams A, Schulze I, et al. Uptake of oxidized lipids by the scavenger receptor CD36 promotes lipid peroxidation and dysfunction in CD8+ T cells in tumors. *Immunity.* 2021;54(7):1561–1577.e7. doi:10.1016/j.immuni.2021.05.003.
39. Shen DD, Pang JR, Bi YP, Zhao L-F, Li Y-R, Zhao L-J, Gao Y, Wang B, Wang N, Wei L, et al. LSD1 deletion decreases exosomal PD-L1 and restores T-cell response in gastric cancer. *Mol Cancer.* 2022;21(1):75. doi:10.1186/s12943-022-01557-1.
40. Zhang Y, Shi J, Liu X, Feng L, Gong Z, Koppula P, Sirohi K, Li X, Wei Y, Lee H, et al. BAP1 links metabolic regulation of ferroptosis to tumour suppression. *Nat Cell Biol.* 2018;20(10):1181–1192. doi:10.1038/s41556-018-0178-0.

41. Kaufman HL, Kohlhapp FJ, Zloza A. Oncolytic viruses: a new class of immunotherapy drugs. *Nat Rev Drug Discov.* 2015;14(9):642–662. doi:10.1038/nrd4663.
42. Shalhout SZ, Miller DM, Emerick KS, Kaufman HL. Therapy with oncolytic viruses: progress and challenges. *Nat Rev Clin Oncol.* 2023;20(3):160–177. doi:10.1038/s41571-022-00719-w.
43. Yu M, Benjamin MM, Srinivasan S, Morin, E.E., Shishatskaya, E.I, Schwendeman, S.P. and Schwendeman, A. Battle of GLP-1 delivery technologies. *Adv Drug Deliv Rev.* 2018;130:113–130. doi:10.1016/j.addr.2018.07.009.
44. Zalevsky J, Chamberlain AK, Horton HM, Karki S, Leung IWL, Sproule TJ, Lazar GA, Roopenian DC, Desjarlais JR. Enhanced antibody half-life improves in vivo activity. *Nat Biotechnol.* 2010;28(2):157–159. doi:10.1038/nbt.1601.
45. Deting Gong MC, Wang Y, Wang Y, Shi J, Hou Y. Juanjuan Shi and Yongzhong Hou: role of ferroptosis on tumor progression and immunotherapy. *Cell Death Discovery.* 2022;8(1):427. doi:10.1038/s41420-022-01218-8.
46. Matsushita M, Freigang S, Schneider C, Conrad M, Bornkamm GW, Kopf M. T cell lipid peroxidation induces ferroptosis and prevents immunity to infection. *J Exp Med.* 2015;212(4):555–568. doi:10.1084/jem.20140857.
47. Xu C, Sun S, Johnson T, Qi R, Zhang S, Zhang J, Yang K. The glutathione peroxidase Gpx4 prevents lipid peroxidation and ferroptosis to sustain Treg cell activation and suppression of antitumor immunity. *Cell Rep.* 2021;35(11):109235. doi:10.1016/j.celrep.2021.109235.
48. Yao Y, Chen Z, Zhang H, Chen C, Zeng M, Yunis J, Wei Y, Wan Y, Wang N, Zhou M, et al. Selenium–GPX4 axis protects follicular helper T cells from ferroptosis. *Nat Immunol.* 2021;22(9):1127–1139. doi:10.1038/s41590-021-00996-0.
49. Chesney JA, Puzanov I, Ross MI, Collichio FA, Milhem MM, Chen L, Kim JJ, Garbe C, Hauschild A, Andtbacka RHI, et al. Primary results from a randomized (1:1), open-label phase II study of talimogene laherparepvec (T) and ipilimumab (I) vs I alone in unresected stage IIIB–IV melanoma. *J Clin Oncol.* 2017;35(15_suppl):9509–9509. doi:10.1200/JCO.2017.35.15_suppl.9509.
50. Antoni Ribas RD, Puzanov I, VanderWalde A, Andtbacka RHI, Michielin O, Olszanski AJ, Malvey J, Cebon J, Fernandez E, Kirkwood JM, et al. Long: oncolytic virotherapy promotes intratumoral T cell infiltration and improves anti-PD-1 immunotherapy. *Cell.* 2017;170(6):1109–1119.e1110. doi:10.1016/j.cell.2017.08.027.